Magic-Angle-Spinning NMR of the Drug Resistant S31N M2 Proton Transporter from Influenza A

ARTICLE *in* JOURNAL OF THE AMERICAN CHEMICAL SOCIETY · APRIL 2012

Impact Factor: 12.11 · DOI: 10.1021/ja3003606 · Source: PubMed

4 AUTHORS, INCLUDING:

Loren B Andreas
Ecole normale supérieure de Lyon
21 PUBLICATIONS **314** CITATIONS
SEE PROFILE

James J Chou
Harvard Medical School
86 PUBLICATIONS **5,349** CITATIONS
SEE PROFILE

Robert G Griffin
Massachusetts Institute of Technology
454 PUBLICATIONS **25,062** CITATIONS
SEE PROFILE

Published in final edited form as:
J Am Chem Soc. 2012 May 2; 134(17): 7215–7218. doi:10.1021/ja3003606.

MAS NMR of the Drug Resistant S31N M2 Proton Transporter from Influenza A

Loren B. Andreas[1], **Matthew T. Eddy**[1], **James J. Chou**[2], and **Robert G. Griffin**[1]

Robert G. Griffin: rgg@mit.edu

[1]Francis Bitter Magnet Laboratory and Department of Chemistry, Massachusetts Institute of Technology, Cam-bridge, Massachusetts 02139, United States

[2]Department of Biological Chemistry and Molecular Pharmacology, Harvard Medical School, Boston, MA 02115, USA

Abstract

We report chemical shift assignments of the drug-resistant S31N mutant of $M2_{18-60}$ determined with magic angle spinning (MAS) 3D spectra acquired with a ^{15}N-^{13}C ZF-TEDOR transfer followed by ^{13}C-^{13}C mixing by RFDR. The MAS spectra reveal two sets of resonances, indicating that the tetramer assembles as a dimer of dimers, similar to the wild type channel. The two sets of chemical shifts are shown to be in close proximity at residue H37, and assignments reveal a difference in the helix torsion angles, as predicted by TALOS+, for the key resistance residue N31. In contrast to wild type $M2_{18-60}$, chemical shift changes are minimal with addition of the inhibitor rimantadine, suggesting that the drug does not bind to S31N.

The M2 proton transporter from Influenza A conducts at low pH and is the target of aminoadamantyl inhibitors rimantadine (Rmt) and amantadine (Amt) whose activity is believed to arise from binding to the pore of the channel.[1–6] The inhibitors reduce the rate of proton conduction, thereby interfering with the unpacking of the viral particle in the endosomal pathway for infection. However, a single mutation from serine 31 to asparagine (S31N) renders these inhibitors ineffective for many current influenza A infections[7] and therefore understanding the structure of the S31N mutant and the structural basis for resistance could guide the design of more potent inhibitors that would target current flu variants. In addition, since the S31N mutation is far more prevalent than the commonly studied Udorn (WT) strain of M2, the structure of S31N M2 is more relevant for the design of novel inhibitors that might exploit a new mechanism.

A segment of the protein comprising residues roughly 18–60 of the full 97 amino acid sequence is known to retain the critical function of proton conduction and inhibition by Amt and Rmt.[8,9] Several structures and structural models of WT M2 have been reported using solution NMR,[10] oriented sample NMR,[5] crystallography,[4] and solid state NMR that combined oriented sample constraints[11] and magic angle spinning (MAS).[12] However, there have been few investigations of the S31N mutant. A solution NMR structure of S31N M2 was reported,[9] but it was solved using a detergent and buffer system that did not support Rmt binding in the pore of WT M2. Thus, it appears that M2 structure and inhibition are sensitive to membrane mimetic environment. Therefore, an investigation of the S31N

SUPPORTING INFORMATION AVAILABLE

Table of TALOS+ predicted torsion angles. Chemical shift assignment table. Spectrum showing the protonation state of H37. ^{13}C-^{13}C spectra at 10 and 30 °C. Peak doubling and drug induced shift change as a function of residue number. Figure 2 with aromatic assignments labeled. This information is available free of charge via the Internet at http://pubs.acs.org/.

variant in fully hydrated lipid bilayers could reveal new functionally relevant structural features.

Additionally, the S31N mutant can be used as a negative control for experiments that investigate the effects of drug binding. It was shown previously that large and widespread chemical shift changes occur upon binding of Rmt to WT $M2_{18-60}$[13] and similar changes occur in a shorter construct comprising residues 22–46.[14] Since S31N $M2_{18-60}$ is drug resistant, chemical shift changes due to nonspecific effects should remain upon addition of drug, and the functionally important chemical shift changes should be absent. Therefore, the S31N mutant can assist in differentiating between binding and non-specific hydrophobic effects that may be present due to a large excess of inhibitor used in the MAS NMR experiments.

Here we report the initial MAS NMR spectra of S31N $M2_{18-60}$ reconstituted into lipid bilayers, from which we derive interesting details of the channel structure. Spectra of S31N $M2_{18-60}$ at 900 MHz (Figure 1) exhibit high resolution of ~0.7 and 0.5 ppm for ^{15}N and ^{13}C backbone linewidths, respectively. This allowed all strong resonances in this ZF-TEDOR[15,16] spectrum to be assigned based on sequence information and sequential correlations in a 3D ^{15}N-^{13}C-^{13}C chemical shift correlation experiment using ZF-TEDOR and RFDR[17,18] (Figures 3–4, assignments in Table S2). Full assignments were made for 14 of the 43 residues, and an additional 7 ^{15}N assignments were made due to transamination of isoleucine and leucine residues such that these residues were ^{15}N labeled despite addition of natural abundance amino acids prior to protein expression (details below). The ^{13}C signal was suppressed for these residues. A second set of resonances of comparable amplitude (denoted with a prime in the figures) was assigned for each residue in the transmembrane region of the peptide between residues 25 and 42, similar to what was observed for WT M2.[13]

This extensive doubling of cross-peaks suggests that the channel assembles as a C_2 symmetric tetramer in a dimer of dimers configuration, rather than a C_4 symmetric tetramer. The C_2 symmetry was previously proposed as the best explanation to WT spectra that also demonstrated similar intensities between the two sets of peaks.[13] Nevertheless, there remained the possibility that the doubled peaks were caused by two different populations of protein that happened to have similar intensity. We exclude the possibility of multiple separate tetramer conformations by showing a cross-peak between the two sets of chemical shifts in a 400 ms PDSD spectrum recorded at 750 MHz (Figure 2, Figure S6). The cross-peak labeled in the figure is between H37 Cδ2 and H37′ Cε1. Since H37 is a pore-facing residue known to play a critical role in ^{1}H selectivity and the pH dependence of ^{1}H conduction,[19,20] we conclude that this cross-peak is within a single tetramer, and not a possible tetramer-tetramer contact. In other parts of the molecule, we do not see analogous cross-peaks, indicating that the two sets of shifts do not exchange on this timescale. We therefore conclude that in lipid bilayers, as opposed to detergent, the protein assembles as a dimer of dimers with C_2 symmetry on the NMR timescale.

Unlike WT M2, only relatively minor changes in chemical shift (<2 ppm ^{15}N, <1 ppm ^{13}C) are observed with addition of a four-fold molar excess of the inhibitor Rmt. Notably, the ~7 ppm change in the ^{15}N shift of residue 31 and the ~3.5 ppm change in the shift for H37 Cα are absent in S31N M2[21]. The largest chemical shift changes occur in lipid facing residues such as V28 Cα and I32 ^{15}N that also lie near the lipid head groups where the amphiphilic Rmt is expected to partition. Since the inhibitor partitions strongly to membranes,[22] it occupies ~7% of the total membrane components by mass (~35 mol %). Therefore the shift changes can be attributed to nonspecific differences in the membrane composition upon addition of drug.

The program TALOS+ was used to predict the backbone torsion angles φ and ψ for both sets of chemical shifts and the results are listed in Table S1 of the supporting information. Since TALOS+ makes predictions based on sequential amino acid triplets, the current labeling restricted the analysis to the longest stretch of continuously labeled and assigned residues 27–31, VVAAN. As expected, the results show an alpha helical conformation. More interestingly, the two sets of chemical shifts are separate enough to show a difference in predicted torsion angles. The predicted values of φ,ψ differ by 13°,14°, respectively for the key resistance residue N31 suggesting that the symmetrically inequivalent helices may have different secondary structures.

The widespread cross-peak doubling and C_2 structure is thus far uniquely resolved for the 18–60 construct in lipid bilayers. In solution, only a single set of resonances was observed, indicating that if two conformations exist, they are exchanging fast on the NMR timescale. This resulted in C_4 symmetric structural constraints.[9] Crystal structures of WT $M2_{22-46}$ showed some conformational heterogeneity, but a C_2 axis was apparently not evident, as channel models based on the crystal structure were constructed with C_4 symmetry.[4] Peak doubling was not resolved by MAS NMR of the shorter construct of WT $M2_{22-46}$,[12] however, doubling may be present beneath the significantly broader line widths that were reported for the 22–46 construct. The dimer of dimers topology is in qualitative agreement with a previous MAS NMR study that proposed an imidazole-imidazolium dimer in $M2_{22-46}$,[19] implying C_2 symmetry at H37. However, at pH 7.8, we observe neutral His (based on sidechain nitrogen shifts near 250 ppm, Figure S1) for both sets of chemical shifts, in contrast with the imidazole-imidazolium dimers that were reported to form when the tetramer is doubly protonated with a pKa of 8.2. Nevertheless, it is possible that the previously reported dimerization and the widespread doubling of peaks are manifestations of the same underlying structural feature and that the pKa is sensitive to the sample differences.

Existing evidence points to several possible modes by which the S31N mutation confers drug resistance. The larger sidechain of asparagine might prevent the drug from binding by reducing the space in the pore, and this mode of resistance was supported by surface plasmon resonance measurements in which binding was not observed for the S31N mutant.[23,24] On the other hand, structures solved by solution NMR show residue 31 in the helix-helix interface,[3,9,10] suggesting that the mutation might severely weaken channel-drug interactions by altering helix packing. The widespread doubling of resonances, and the 13°, 14° difference in the predicted value of φ,ψ for N31 suggest that detailed understanding of the drug resistant structure may include twofold channel symmetry.

Chemical shift assignments were achieved via 3D ^{15}N-^{13}C-^{13}C spectra [25,26] using one bond ^{15}N-^{13}C ZF-TEDOR mixing followed by ^{13}C-^{13}C RFDR mixing, similar to previously described 2D experiments[27] and the commonly used N-C cross-polarization (DCP) based experiments.[28–31] The sequence is depicted in Figure 3 and allows both the NCOCX and NCACX connectivity experiments to be efficiently acquired in a single spectrum (Figure 4). Efficient NCACX and NCδCX transfers are demonstrated for Pro, a residue that is often difficult to observe in DCP spectra due to weak H-N cross-polarization to the Pro nitrogen. The ZF-TEDOR transfer avoids this problem because the experiment begins with an H-C cross-polarization step. In principle, this experiment should also provide assignment information originating from sidechain ^{15}N's in residues such as histidine, tryptophan, lysine, and arginine. However, we found that these transfer efficiencies were reduced and their detection would have required significantly longer experiment times. In order to avoid excessive spectral widths in the indirect ^{13}C dimension, we folded the carbonyl resonances onto the spinning side band just higher than the aliphatic resonances, by applying a dwell time matching the rotor period. A spinning frequency corresponding to ~90 ppm was useful

for this reduction in the sweep width, and also avoids strong rotational resonance conditions.[32–34]

$M2_{18-60}$ was prepared by over expression in E. Coli as described previously[10,13] with C19S and C50S mutations to prevent unwanted disulphide bond formation. The resulting sequence with the S31N mutation was RSNDSSDPLV VAANIIGILH LILWILDRLF FKSIYRFFEH GLK. In order to simplify the spectra, residues ILFY were unlabeled by addition of the natural abundance amino acids to the culture approximately 1 hour prior to induction. Bilayer protein samples were prepared by adding 1,2-di-O-phytanoyl-*sn*-glycero-3-phosphocholine (DPhPC) lipid (Avanti) and lyophilized $M2_{18-60}$ at a lipid to protein ratio of 1:1 by weight (~6:1 by mol) both dissolved in denaturing buffer (6M guanidine, 40 mM phosphate, 30 mM glutamate, 3 mM sodium azide (Sigma-Aldrich), pH 7.8, >=33mg/mL OG detergent (Anatrace)). The resulting solution was dialyzed in a 3.5kD cutoff dialysis cassette (Thermo) against 1 L of sample buffer (40 mM phosphate, 30 mM glutamate, 3 mM sodium azide, pH 7.8) for 7 days with 2 dialysis buffer changes per day. A white precipitate was observed after approximately 24 hours. Solid membrane material was pelleted by centrifugation at ~100,000 × g. Samples with rmt had a four-fold molar excess added directly to the membrane pellet.

The NMR spectrum in Figure 2 was recorded on a 750 MHz spectrometer courtesy of David Ruben and all other spectra were recorded using a Bruker 900 MHz spectrometer (Bruker Biospin). Each instrument employed a Bruker 3.2 mm HCN e-free probe. Referencing was performed using the chemical shifts of adamantine relative to DSS for ^{13}C[35] and the relative frequency ratios between DSS (^{13}C) and liquid ammonia (^{15}N)[36,37] for ^{15}N referencing. The sample temperature was estimated using the chemical shift of ^{79}Br in KBr to determine heating due to sample spinning.[38] (See Figure S2 for a comparison of spectra recorded at 10 and 30 °C, the temperatures used for PDSD and assignment, respectively) Spectra were processed with NMRPipe[39] and displayed and assigned using Sparky (Goddard and Kneller, University of California, San Francisco).

We have shown that a single 3D ZF-TEDOR-RFDR spectrum acquired in 5 days is sufficient for sequential assignment of reverse ILFY labeled S31N $M2_{18-60}$. Minor differences in chemical shift were observed upon addition of inhibitor, and the absence of dramatic shift changes seen for WT M2 confirm their functional significance. The assignments revealed two distinct sets of resonances that are shown to be in close contact using PDSD mixing from which we conclude that the tetramer assembles as a dimer of dimers with C_2 symmetry and two symmetrically inequivalent helices. The predicted TALOS+ geometry of the two helices is also found to be distinct, particularly for the resistance residue N31. These structural features observed in lipid bilayers provide clues to the mechanism of resistance, and further structural investigation of drug resistant M2 could provide a starting point for the design of more potent or novel inhibitors.

Supplementary Material

Refer to Web version on PubMed Central for supplementary material.

Acknowledgments

This work was supported by grants EB-001960, EB-002026, AI-067438 and GM-094608. We thank Rafal Pielak and Marcelo Berardi for thoughtful discussions.

References

1. Cady SD, Schmidt-Rohr K, Wang J, Soto CS, DeGrado WF, Hong M. Nature. 463:689. [PubMed: 20130653]
2. Jing X, Ma C, Ohigashi Y, Oliveira FA, Jardetzky TS, Pinto LH, Lamb RA. Proc Natl Acad Sci U S A. 2008; 105:10967–72. [PubMed: 18669647]
3. Pielak RM, Oxenoid K, Chou JJ. Structure. 2011; 19:1655–63. [PubMed: 22078564]
4. Stouffer AL, Acharya R, Salom D, Levine AS, Di Costanzo L, Soto CS, Tereshko V, Nanda V, Stayrook S, DeGrado WF. Nature. 2008; 451:596–9. [PubMed: 18235504]
5. Sharma M, Yi M, Dong H, Qin H, Peterson E, Busath DD, Zhou HX, Cross TA. Science. 2010; 330:509–12. [PubMed: 20966252]
6. Yi M, Cross TA, Zhou HX. Journal of Physical Chemistry B. 2008; 112:7977–7979.
7. Bright RA, Shay DK, Shu B, Cox NJ, Klimov AI. JAMA. 2006; 295:891–4. [PubMed: 16456087]
8. Ma C, Polishchuk AL, Ohigashi Y, Stouffer AL, Schon A, Magavern E, Jing X, Lear JD, Freire E, Lamb RA, DeGrado WF, Pinto LH. Proc Natl Acad Sci U S A. 2009; 106:12283–8. [PubMed: 19590009]
9. Pielak RM, Schnell JR, Chou JJ. Proc Natl Acad Sci U S A. 2009; 106:7379–84. [PubMed: 19383794]
10. Schnell J, Chou J. Nature. 2008; 451:591–595. [PubMed: 18235503]
11. Hu J, Asbury T, Achuthan S, Li C, Bertram R, Quine JR, Fu R, Cross TA. Biophys J. 2007; 92:4335–43. [PubMed: 17384070]
12. Cady SD, Schmidt-Rohr K, Wang J, Soto CS, Degrado WF, Hong M. Nature. 2009; 463:689–92. [PubMed: 20130653]
13. Andreas LB, Eddy MT, Pielak RM, Chou J, Griffin RG. J Am Chem Soc. 132:10958–60. [PubMed: 20698642]
14. Cady SD, Mishanina TV, Hong M. J Mol Biol. 2009; 385:1127–41. [PubMed: 19061899]
15. Jaroniec CP, Filip C, Griffin RG. J Am Chem Soc. 2002; 124:10728–42. [PubMed: 12207528]
16. Hing AW, Vega S, Schaefer J. Journal of Magnetic Resonance. 1992; 96:205–209.
17. Bennett AE, Ok JH, Griffin RG, Vega S. Journal of Chemical Physics. 1992; 96:8624–8627.
18. Bennett AE, Rienstra CM, Griffiths JM, Zhen WG, Lansbury PT, Griffin RG. Journal of Chemical Physics. 1998; 108:9463–9479.
19. Hu J, Fu R, Nishimura K, Zhang L, Zhou HX, Busath DD, Vijayvergiya V, Cross TA. Proceedings of the National Academy of Sciences of the United States of America. 2006; 103:6865–6870. [PubMed: 16632600]
20. Wang C, Lamb RA, Pinto LH. Biophys J. 1995; 69:1363–71. [PubMed: 8534806]
21. Cady SD, Luo W, Hu F, Hong M. Biochemistry. 2009; 48:7356–7364. [PubMed: 19601584]
22. Wang JF, Schnell JR, Chou JJ. Biochemical and Biophysical Research Communications. 2004; 324:212–217. [PubMed: 15465004]
23. Astrahan P, Kass I, Cooper MA, Arkin IT. Proteins-Structure Function and Bioinformatics. 2004; 55:251–257.
24. Rosenberg MR, Casarotto MG. Proceedings of the National Academy of Sciences of the United States of America. 2010; 107:13866–13871. [PubMed: 20643947]
25. Sun BQ, Rienstra CM, Costa PR, Williamson JR, Griffin RG. J Am Chem Soc. 1997; 119:8540–8546.
26. Rienstra CM, Hohwy M, Hong M, Griffin RG. J Am Chem Soc. 2000; 122:10979–10990.
27. Riedel K, Leppert J, Ohlenschlager O, Gorlach M, Ramachandran R. J Biomol NMR. 2005; 31:49–57. [PubMed: 15692738]
28. Ladizhansky V, Jaroniec CP, Diehl A, Oschkinat H, Griffin RG. Journal of the American Chemical Society. 2003; 125:6827–6833. [PubMed: 12769594]
29. Rienstra CM, Hohwy M, Mueller LJ, Jaroniec CP, Reif B, Griffin RG. J Am Chem Soc. 2002; 124:11908–22. [PubMed: 12358535]

30. Sun BC, Rienstra CM, Costa JR, Williamson JR, Griffin RG. J Am Chem Soc. 1997; 119:8540–8546.
31. Castellani F, van Rossum BJ, Diehl A, Rehbein K, Oschkinat H. Biochemistry. 2003; 42:11476–11483. [PubMed: 14516199]
32. Raleigh DP, Harbison GS, Neiss TG, Roberts JE, Griffin RG. Chemical Physics Letters. 1987; 138:285–290.
33. Raleigh DP, Levitt MH, Griffin RG. Chemical Physics Letters. 1988; 146:71–76.
34. Levitt MH, Raleigh DP, Creuzet F, Griffin RG. Journal of Chemical Physics. 1990; 92:6347–6364.
35. Morcombe CR, Zilm KW. J Magn Reson. 2003; 162:479–86. [PubMed: 12810033]
36. Markley JL, Bax A, Arata Y, Hilbers CW, Kaptein R, Sykes BD, Wright PE, Wuthrich K. J Biomol NMR. 1998; 12:1–23. [PubMed: 9729785]
37. Harris RK, Becker ED, Cabral de Menezes SM, Goodfellow R, Granger P. Solid State Nucl Magn Reson. 2002; 22:458–483. [PubMed: 12637147]
38. Thurber KR, Tycko R. Journal of Magnetic Resonance. 2009; 196:84–87. [PubMed: 18930418]
39. Delaglio F, Grzesiek S, Vuister GW, Zhu G, Pfeifer J, Bax A. J Biomol NMR. 1995; 6:277–93. [PubMed: 8520220]

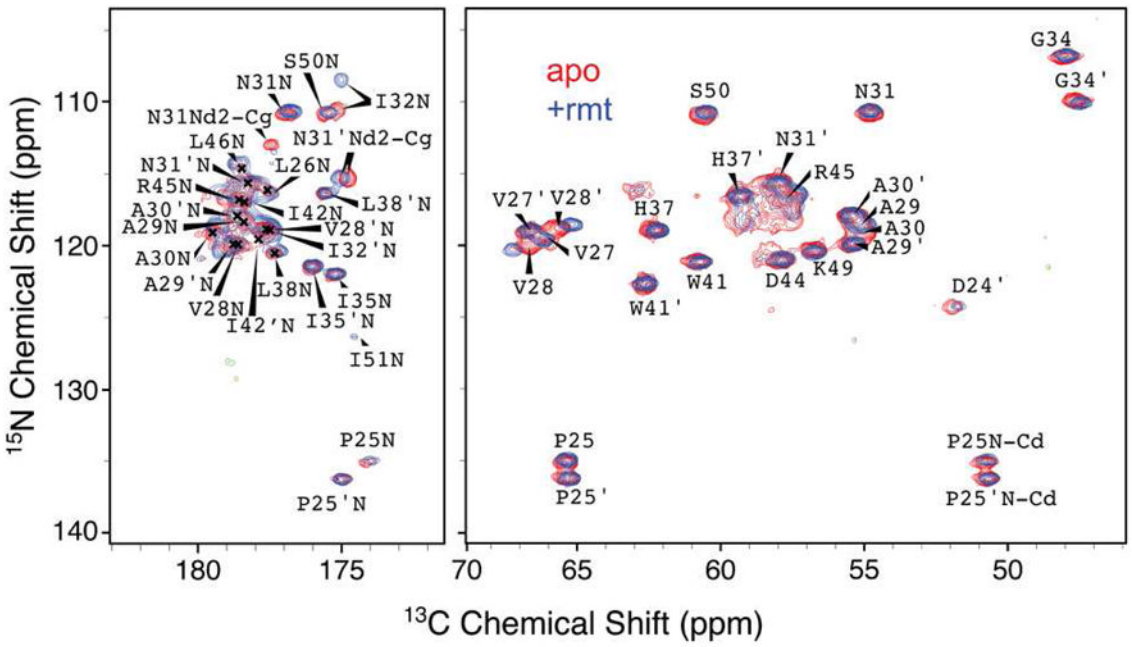

Figure 1.

ZF-TEDOR spectra of S31N $M2_{18-60}$ are shown in the presence (blue) and absence (red) of the inhibitor Rmt. Spectra were recorded at a ^{1}H frequency of 900 MHz and demonstrate ~0.7 ppm and ~0.5 ppm ^{15}N and ^{13}C backbone linewidths, respectively. Labels correspond to N-Cα cross-peaks (right) and nitrogen i of N_i-C_{i-1} cross-peaks (left) unless otherwise indicated. The sample temperature was ~30 °C, the spinning frequency was 20 kHz, and the TEDOR mixing time was 1.2 ms.

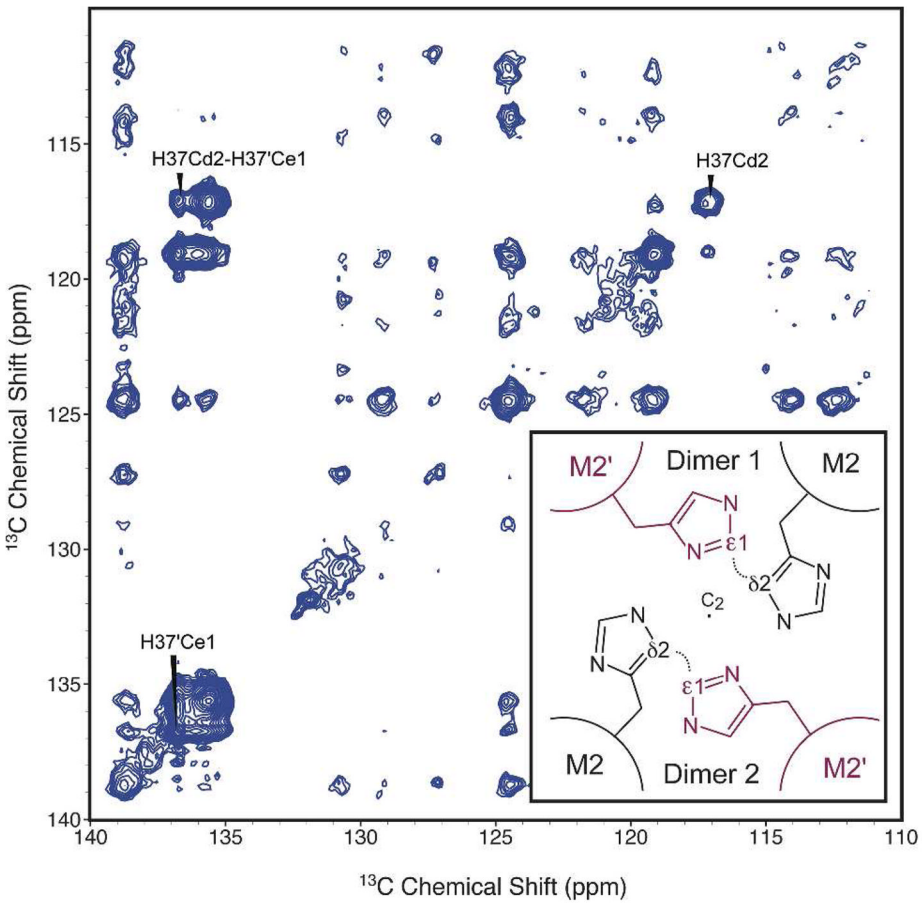

Figure 2.

An aromatic-aromatic ^{13}C correlation spectrum using 400 ms of proton driven spin diffusion mixing shows cross-peaks between the two sets of chemical shifts. The sample temperature was ~10 °C and the spinning frequency was 14.287 kHz. The inset shows an illustration of a C_2 symmetric channel composed of a dimer of dimers viewed along the C_2 axis with the four alpha helices at the corners. The observed intermolecular correlation between carbons δ2 and ε1′ is also depicted in the inset.

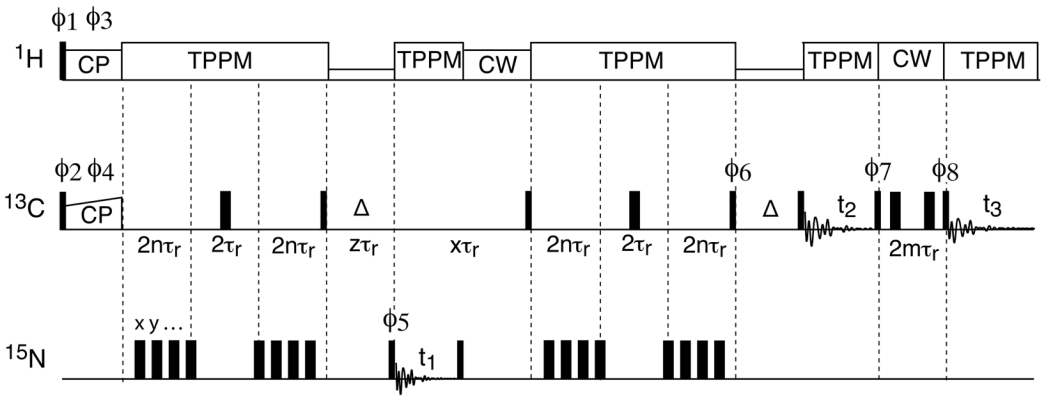

Figure 3.

3D ZF-TEDOR-RFDR pulse sequence used for assignments. Narrow and broad bars represent pulses of 90 and 180 degree nutation respectively. Vertical dashed lines indicate rotor synchronization. The parameter n determines the total TEDOR mixing time, and the parameter m likewise determines the RFDR mixing, by extension of the respective pulse trains. The phase cycle was φ_1=(16×1)(16×3), φ_2=(16×4)(16×2), φ_3=2, φ_4=1, φ_5=13, φ_6=2244, φ_7=1133, φ_8=1111222233334444, φ_{rec}=4242 1313 2424 3131 2424 3131 4242 1313. The REDOR mixing in ZF-TEDOR used xy-4, and the RFDR mixing used xy-16 phase alternation. All other pulses had a phase of 1. The phases of the pulses after t_1 evolution and before t_2 evolution were incremented for phase sensitive detection. Due to time constraints, only the first 4 values of the phase cycle were used.

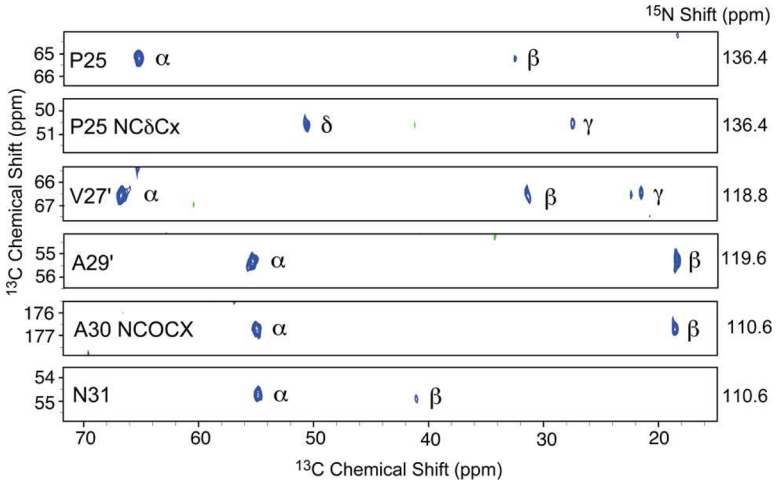

Figure 4.

Slices are shown from the NCACX and NCOCX regions of a 3D ZF-TEDOR-RFDR spectrum used for sequential assignments. For P25, the NCδ transfer was also efficient (second panel). 1.2 ms of TEDOR mixing and 4.8 ms of RFDR mixing with 83 kHz pulses were used. The direct acquisition used a 6 μs dwell time and 3072 points (~18.4 ms), the indirect ^{13}C dimension was acquired with a 50 μs dwell time and 180 complex points (9 ms), and the ^{15}N dimension used a 150 μs dwell time and 74 complex points (11.1 ms). The carrier frequency was set to 100 ppm for ^{15}N, and 89 ppm for ^{13}C. The spectrum was acquired in ~5 days and provided useful NCACX and NCOCX connectivity information. The sample temperature was ~30 °C, and the spinning frequency was 20 kHz.